Journal of Solid State Electrochemistry
https://doi.org/10.1007/s10008-024-05962-y

ORIGINAL PAPER

Central composite rotatable design for non-convex optimization of removal efficiency of hydroxychloroquine in an electrochemical cell

Alejandro Regalado-Méndez[1] · Daniel Vásquez-Hernández[1] · Reyna Natividad[2] · Ever Peralta-Reyes[1]

Received: 8 March 2024 / Revised: 24 May 2024 / Accepted: 4 June 2024

Abstract

Hydroxychloroquine sulfate (HCQ), an against-COVID-19 drug, is a dangerous organic compound in wastewater. In this study, 0.6 L of an HCQ solution (50 mg L^{-1}) was electro-oxidized in a batch electrochemical cell (BEC) with two boron-doped diamond (BDD) electrodes. The optimal operating conditions were established by DoE-driven non-convex constrained optimization. A central composite rotatable design (CCRD) was applied to model the chemical oxygen demand (COD) removal efficiency and to evaluate the influence of current density (j): 10–120 mA cm^{-2}, initial pH: 2–12, and stirring speed (Ω): 400–600 rpm. Experimental results were modeled by a reduced third-order polynomial function having a determination coefficient (R^2), root mean square error (RMSE), mean square error (MSE), and coefficient of variation (C.V.) of 0.9906, 0.0460, 0.0021, and 3.72%, respectively. This validates the predictive capacity of the fitted model and the efficiency of the employed electro-oxidation process. The optimal operating vector was $j = 46.36$ mA cm^{-2}, $pH_0 = 12.04$, and $\Omega = 584$ rpm within 5 h of reaction time, attaining a maximum COD removal efficiency of 85.55% with an energy consumption of 1.24 kW h L^{-1} and a total operating cost of 0.067 USD$ L^{-1}. Also, a total organic carbon removal of 52.5% was achieved. Additionally, mathematical models were established to fit the temporary profiles of HCQ degradation, COD, and TOC removal. The estimated apparent kinetic constants (k_{app}) were 1.21 h^{-1}, 0.26 h^{-1}, and 2.65 mg L^{-1} h^{-1}, respectively. Finally, it was concluded that the assessed electrochemical process could help mineralizing wastewater containing HCQ.

Keywords Batch electrochemical cell · BDD electrode · Electrochemical degradation · Hydroxychloroquine · Non-convex optimization

Nomenclature

a	Electrode surface (cm^2)
ANOVA	Analysis of variance
BDD	Boron-doped diamond
BEC	Batch electrochemical cell
C	Concentration (mg L^{-1})
CCD	Central composite design
CCRD:	Central composite rotatable design
COD	Chemical oxygen demand (mg L^{-1})
C.V.	Coefficient of variation (%)
EC	Total energy consumption (kW h)
E	Electricity used (kW h)
F-value	Ratio of the mean square's treatment to the mean squares error
GWE	Global warming potential
HCQ	Hydroxychloroquine
j	Current density (mA cm^{-2})
i	Current intensity (μA)
K	Factor number
k	Kinetic constant (h^{-1})
m	Mass of electrolyte (kg)
MSE	Mean square error
$OH^{\bullet}$	Hydroxyl radical
OC	Operating cost (USD$)
pH	Power of hydrogen (dimensionless)
p-value:	Probability of getting a result at least as extreme as the one that was observed
P	Supplier catalog nominal power (kW h)
RMSE	Root mean square error
R^2	Determination coefficient

✉ Alejandro Regalado-Méndez
alejandro.regalado33@gmail.com

✉ Ever Peralta-Reyes
e_pere70@hotmail.com

[1] Research Laboratories, Universidad del Mar-Campus Puerto Ángel, Ciudad Universitaria, Col. El Faro, Puerto Ángel, San Pedro Pochutla 70902, México

[2] Chemical Engineering Laboratory, Joint Centre for Research on Sustainable Chemistry, UAEM-UNAM, Universidad Autónoma del Estado de México, Km 14.5 Toluca-Atlacomulco Road, Toluca 50200, México

Published online: 13 June 2024

t	Electrolysis time (h)
TOC	Total organic carbon (mg L^{-1})
T	Temperature (°C)
U	Mean voltage cell (V)
V	Volume treated (L)
VIFs	Variance inflation factor
x	Encrypted independent variables

Greek letters

α	Rotatability (1.68)
γ	Values of the coefficient of the polynomial equation
Δ	Increased
ξ	Electricity price (USD$ (kW h)$^{-1}$)
Ω	Stirred speed (rpm)
η	Efficiency (%)
ϕ	Electrolyte price (USD$ kg^{-1})

Suffixes

Adj	Adjusted
app	Apparent
Elec	Electrode
Model	Model
M	Mineralization
Pred	Predicted
Pump	Recirculation pump
Stirred	Magnetic stirred
Tr	Treated
i	Number of independent variables
0	Initial

Introduction

Even though industrialization improves the economy worldwide and makes some tasks easier for humans, this anthropogenic activity causes serious water contamination problems. Also, the COVID-19 pandemic period exhibits a critical relevance regarding water sanitation since many drugs (e.g., chloroquine, hydroxychloroquine (HCQ), remdesivir, ivermectin, and azithromycin) were consumed to counteract the COVID-19 virus. HCQ is used as a treatment against malaria, lupus, arthritis [1], and COVID-19 because of its potent antiviral properties with a dosage of 600 mg daily [2]. This has caused an increase in medical prescriptions and consequently an input increase of these pharmaceutical drugs into the water bodies through wastewater discharges from the pharmaceutical industry (10 to 1000 times higher than other effluents), hospital wastes, wastewater treatment plants, and human waste [3]. In this context, Agenda 2030 through the Sustainable Development Goals (Objective 6. Clean water and sanitation) [4] adopted by all United Nations Member States mentions that the decontamination of wastewater is worldwide one of the priority targets since water is a vital liquid to maintain life on our planet. However, conventional wastewater treatment plants (WWTP) are not able to efficiently remove pharmaceutical drugs [5]. In the specific case of HCQ, the WWTP has low degradation efficiency (approximately 6%) because of its low biodegradability and hydrophilicity (Log (K_{OW}) < 3) [6]. Because of its chemical and biological characteristics, HCQ tends to persist, bioaccumulates, is carcinogenic, and transfer inside of aquatic organisms causing an intensified toxicity [7]. Given the potential risks of against COVID-19 drugs (e.g., HCQ) for living aquatic organisms, it is necessary to implement technologies more effective to accomplish the removal of drugs from water bodies.

Advanced oxidation processes (AOPs) are worldwide acknowledged because of their green characteristics, versatility, amenability to automation, and simplicity in removing persistent organic compounds [8, 9]. Particularly, anodic oxidation by using boron-doped diamond (BDD) is based on the direct oxidation of organic pollutants mainly by hydroxyl radicals ($OH^{\bullet}$ with an oxidation potential of 2.8 V) and other oxidizing species (e.g., H_2O_2, O_3, $S_2O_8^{2-}$, and $SO_4^{\bullet-}$) generated on the electrode surface through water oxidation [10, 11]. BDD electrode might be the most suitable anode to perform the electrochemical degradation of persistent organic pollutants since exhibits electrochemical stability, long life, wide potential windows, and organic matter removal efficiencies superior to 95% [12, 13]. However, has the limitation of the cost of production against this, new and novel anode materials (e.g., Ti–Sn/γ-Al_2O_3, Ti/RuO_2–IrO_2, DSA/Pt, DSA-Cl_2, among others) were developed with an organic matter removal efficiency superior to 69% can be utilized [14–17].

The advanced oxidation process can be conducted by different cell configurations; batch cell [18], continuous stirred tank [16], plug-flow [19, 20], flow-by [21, 22], flow-through [23, 24], and others [25–27] have been successfully implemented. In lab-scale studies, a batch cell consisting of two vertical electrodes in an agitated tank is convenient due to the following benefits [8, 28]: i) easy and secure electrical connection, ii) easy incorporation of the electrolyte, iii) easy electrode insertion and removal, iv) appropriate mixing by a magnetic stirring bar, v) possible kinetic analysis of water treatment, and vi) easy continuous pH adjustment.

Once a particular combination of electrodes and electrochemical cell has been elected, it is of paramount importance to establish optimum operating conditions to generate oxidant species, mainly the hydroxyl radical [29]. Conducting this at bench scale is the first step to establish the feasibility of a process to be implemented at a large scale. The optimal conditions can be used not only for the scaling-up of the process but also to establish through life cycle analysis its environmental impacts, like carbon footprint (global warming potential, GWE) [30].

In the context of optimization, the response surface methodology (RSM) stands out as the most popular because of its simplicity and flexibility in the use of experimental designs (e.g., Doehlert, Box-Behnken, central composite rotatable (CCR), Plackett–Burman, among others). The CCR design is the most useful since the number of experiments employed offers enough information to model responses by a polynomial equation as a function of operating parameters. Another important methodology that can be used to optimize electrochemical plants is convex optimization. However, convex optimization has not been enough exploited yet despite being largely employed by environmental and chemical engineering students and of course industrial and academic researchers because there is limited literature focusing on convex optimization of electrochemical plant parameters such as the landfill leachate reverse osmosis (RO) concentration [31], electro-Fenton oxidation of cooking wastewater [32], and chloroquine electro-oxidation [33]. Although convex optimization is a powerful tool, it is limited to optimizing linear and quadratic functions with linear or/and quadratic constraints imposed on a decision-space since some responses could be modeled by third-order polynomial equations (e.g., [34, 35]) or other functions derived from a real-world optimization problem [36]. In this context, the non-convex constrained optimization solves the mentioned limitation by applying the trust-region [37], active-set [38], and sequential quadratic programming [39] methods. These methods have been included in the MATLAB *Toolbox* libraries ("fmincon" function), which works for convex and non-convex-constrained optimization problems.

Table 1 summarizes the efforts of some research groups on assessing the degradation of HCQ by different treatments under different reaction environment conditions, i.e., applying gamma radiation, with UV light, electro-oxidation, or with a combination of the last two. It can be observed in Table 1 that a high degradation efficiency of HCQ is generally achieved; however, the TOC and COD removal efficiencies were not reported in all cases. Also, it can be noted that the optimization of different degradation treatments has not been implemented and the electro-oxidation of HCQ has not been assessed with two BDD electrodes.

The objective of this work was the maximization of the removal of hydroxychloroquine (HCQ) by electro-oxidation in a batch electrochemical cell (BEC) equipped with two BDD electrodes, which was evaluated in terms of the COD removal efficiency (η_{COD}) by the non-convex-constrained optimization method. To accomplish the optimization objective, a CCRD and non-convex constrained optimization was employed to model and evaluate the effect on COD removal efficiency (η_{COD}) by three operating factors, specifically the current density (j), initial power hydrogen (pH_0), and stirring speed (Ω). Additionally, model verification, operating cost, and kinetic rate models for degradation of HCQ, COD, and TOC removal were obtained.

Materials and methods

Chemical substances and aqueous hydroxychloroquine solution

Sulfuric acid (H_2SO_4, purity of 95%) and sodium hydroxide (NaOH, purity of 97%) were from Sigma-Aldrich Company, while hydroxychloroquine sulfate (HCQ, grade standard) and the sodium sulfate (Na_2SO_4, purity of 99%) were purchased from Karal Group (Mexican Company) and Supelco Company, respectively.

An aqueous solution of HCQ (50 mg L^{-1}) with 0.1 M of Na_2SO_4 as supporting electrolyte was prepared in a volumetric flask for each trial. The aqueous solution was

Table 1 Degradation of HCQ by different treatments

Process/Cell	O	NO	Operating environment conditions	Main results		Ref
				η_{HCQ} (%)	η_{TOC} (%)	
GR/Micro batch	–-	x	C_{HCQ} = 20 mg L^{-1}, gamma dosage of 1 kGy, pH_0 = 6.8, 0.6 h	98	–-	[40]
Ph/Batch	–-	x	pH_0 = 6.43, C_{HCQ} = 15.5 mg L^{-1}, 320 mg L^{-1} of bicarbonate, λ = 300–800 nm, 10 h, V = 0.2 L	100	–-	[7]
PhC/Batch	–-	x	C_{HCQ} = 10 mg L^{-1}, pH_0 = 7.5, radiation UV-A, C_{cat} = 20 g L^{-1} of 15%ZnOCP, V = 0.25 L	96	–-	[41]
EO/Flow	–-	x	j = 20 mA cm^{-2}, C_{HCQ} = 125 mg L^{-1}, pH_0 = 7.1, T = 25 °C, 0.05 M Na_2SO_4, EC = 102 kW m^{-3}, 4 h, V = 0.6 L	100	80	[42]
EO-UV/Flow	–-	x	C_{HCQ} = 125 mg L^{-1}, pH_0 = 7.1, UV lamp mercury, λ = 254 nm, 15 W, EC = 63 kW m^{-3}, 4 h, V = 0.6 L	36	–-	
EO-S/Flow	–-	x	C_{HCQ} = 125 mg L^{-1}, pH_0 = 7.1, 9.0 W, EC = 101 kW m^{-3}, 4 h, V = 0.6 L	100	–-	

O Optimized, *NO* Not optimized, *EO* Electrooxidation, *EO-S*, Electrooxidation assisted with sonication, *EO-UV* Electrooxidation assisted with UV radiation; *PhC*: Photocatalyst, Ph Photolysis, *GR* Gamma radiation, *EC* Energy consumption

homogenized for 10 min in a BEC. The pH of aqueous solution was adjusted with a solution either of 0.1 M of NaOH or 0.1 M of H_2SO_4. Additionally, distilled water was employed for preparing all aqueous solutions of HCQ. Table 2 displays the physical–chemical properties of HCQ.

Potentiodynamic polarization measurements

The micro-electrolysis test was carried out using an Autolab potentiostat/galvanostat ® 30 that was controlled with GPE software V 4.3, which consists of a three-electrode cell (volume capacity of 100 mL), using Ag/AgCl, graphite bar, and a BDD electrode (with a geometric area of 1 cm^2) as reference, auxiliary, and working electrodes, respectively. Linear and cyclic voltammetry was as follows: scan rate of 50 mV s^{-1}, range from 0 to 2 V, pH of 5.98, pressure of 1 atm, temperature of 25 °C, and stirring time of 60 s before each voltametric experiment to achieve a homogeneous mixture.

Electrolysis set-up

The electrolysis system (see Fig. 1) was constituted by a BEC (1 L), two BDD electrodes (geometric area of 20 cm^2) separated from each other by 1 cm (only one side of the electrodes contains boron-doped diamond (BDD), and a magnetic stirrer (2 cm). Also, the energy was supplied by using a GW Instek GPR-3510HD D.C. power supply. All experiments were conducted at 25 °C and 1 atm. Cold water was recirculated with a peristaltic pump through the cooling jacket of the cell to maintain the solution at 25 °C. It is worth mentioning the electrode section outside the liquid was insulated with Teflon tape to achieve uniform distribution in potential and current across the BDD electrodes.

Experimental design

An aqueous HCQ solution (0.6 L) was added into the BEC of the electrolysis set-up above described (see Fig. 1). The studied operating factors were current density (j), initial power of hydrogen (pH_0), and stirring speed (Ω), according

Table 2. Solution characteristics and physicochemical properties of HCQ [43], [44], [45]

Formula of HCQ	**Solution characteristics**				
	C_{HCQ} (mg L^{-1})	**pH**	**Conductivity (µS cm^{-1})**	**Turbidity (NTU)**	**COD (mg L^{-1})**
	50	8.3 *	13,310 *	0.34 *	141 *
	Physicochemical properties				
	Property			**Value**	
	Molar weight (g mol^{-1})			433.95	
	Melting point (ºC)			90 [43]	
	Solubility in water (mg mL^{-1}) at 25 ºC			87 [44]	
	Log (K_{ow})			3.03 [6]	
	λ_{Max} (nm)			343 [45]	

Condensed formula:
$C_{18}H_{26}ClN_3O \bullet H_2SO_4$
CAS No.: 747-36-4

* Average value of the trials.

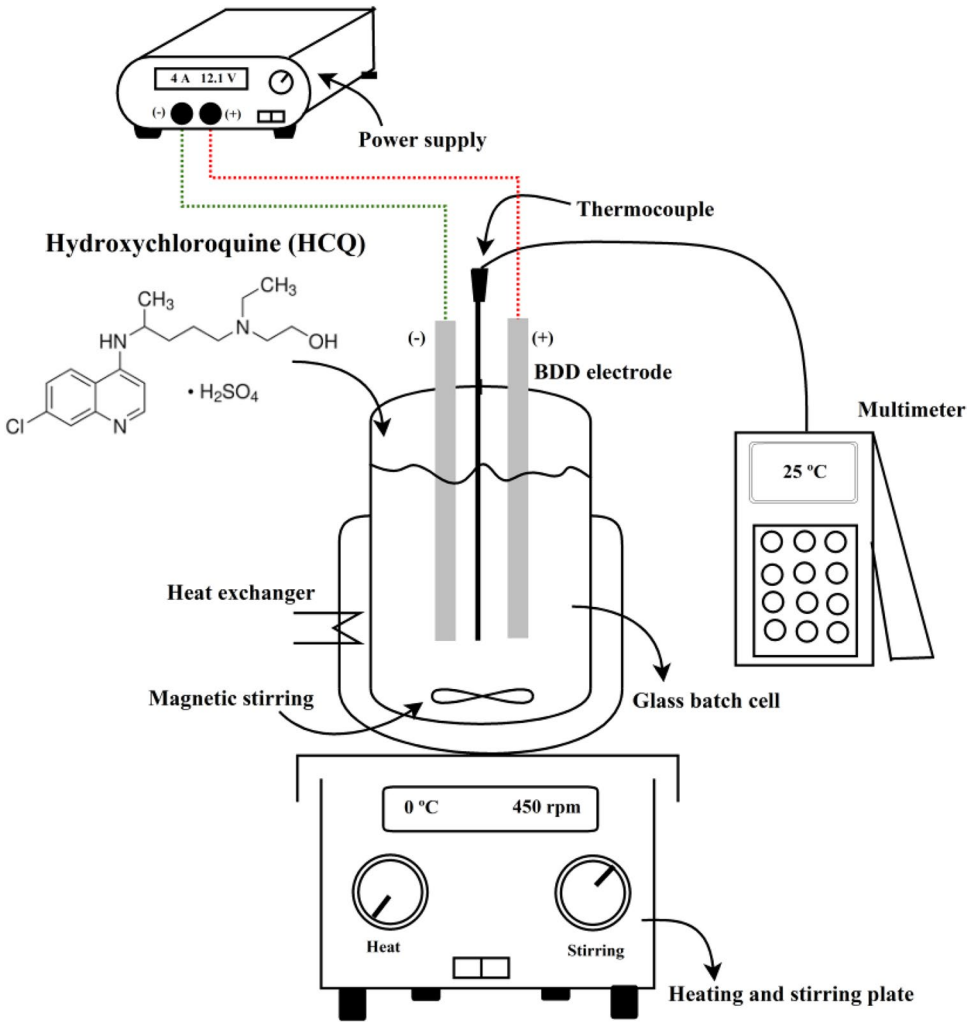

Fig. 1 Electrolysis set-up

Table 3 CCRD design and encoded levels of each operating factor

K operating factors	Levels				
	$-\alpha$	−1	0	+1	$+\alpha$
X_1: j (mA cm^{-2})	10.0	32.5	64.5	96.5	120.0
X_2: pH_0	2.0	4.5	7.0	9.5	12.0
X_3: Ω (rpm)	400	450	500	550	600

to Table 3. The lower, center, upper, and axial levels of each operating factor that appear in Table 3 are encrypted as $-\alpha, -1, 0, +1$, and $+\alpha$, correspondingly according to Eq. (1).

$$x_i = \frac{X_i - X_{i,0}}{\Delta X_i} \quad (1)$$

The design matrix and experiments to perform the optimization of the COD removal efficiency (η_{COD}) are displayed in Table S1. A central composite rotatable design (CCRD with three factors) was adopted as an experimental design. The CCRD was composed of 2^K factorial points, K central points, and 2 K axial points, giving a total of 17 tests. The CCRD and posterior model fit, and ANOVA analysis were conducted using the Design Expert ® V.10.0 software package (serial number: 9839–2917-5744–6919; Multion Consulting, S.A. de C.V, Calz, Mexico from Stat-Ease, Inc.). In this study, the j was selected according to the typical range of current density used in electrochemical removal processes [46], the pH_0 was elected according to the solubility of the HCQ, and the Ω was chosen according to previous author works, where 4-chlorophenol has been electrochemically removed in the same BEC [47].

Chemical analysis

Samples of HCQ solution electrochemically treated for 5 h were taken from BEC. The determination of COD of HCQ solution before and after electrochemical treatment was measured by the Standard Method (5220B) established by

Baird et al. [48]. The COD analysis consists of the complete organic matter oxidation into carbon dioxide with potassium dichromate under acidic conditions (sulfuric acid). Meanwhile, the determination of the TOC of HCQ solution before and after treatment was conducted in a 6001 TOC analyzer Shimadzu, where the TOC analysis consists of the complete oxidation of organic carbon contents in the water sample into carbon dioxide by combustion at high temperatures (680–900 °C) in the presence of platinum or palladium as a catalyst. Additionally, the UV–Vis absorption spectrum of HCQ was detected by using a Lamda 365 PerkinElmer UV–visible spectrophotometer, and the abatement of HCQ during electrochemical treatment was detected at λ_{Max} of 343 nm. Finally, the pH of all HCQ solutions was determined by a HI2210 Hanna potentiometer.

Analytical procedures

The COD degradation efficiency of HCQ (η_{COD}) was determined by the difference in COD quantity between the initial sample and the treated sample, computed by using Eq. (2),

$$\eta_{COD} = \frac{C_{COD,0} - C_{COD,t}}{C_{COD,0}} \times 100 \tag{2}$$

where $C_{COD,\,0}$ and $C_{COD,\,t}$ (mg L^{-1}) is the chemical oxygen demand (COD) of the HCQ solution at times 0 and t, respectively.

The TOC degradation efficiency of HCQ (η_{TOC}) was determined by the difference in TOC quantity between the initial sample and the treated sample according to Eq. (3),

$$\eta_{TOC} = \frac{C_{TOC,0} - C_{TOC,t}}{C_{TOC,0}} \times 100 \tag{3}$$

where $C_{TOC,\,0}$ and $C_{TOC,\,t}$ (mg L^{-1}) is the total organic carbon (TOC) of the HCQ solution at times 0 and t, respectively.

The degradation efficiency of HCQ (η_{HCQ}) was determined by the difference in HCQ quantity between the initial sample and the treated sample according to Eq. (4),

$$\eta_{HCQ} = \frac{C_{HCQ,0} - C_{HCQ,t}}{C_{HCQ,0}} \times 100 \tag{4}$$

where *CHCQ, 0* and *CHCQ, t* (mg L^{-1}) is the concentration of the HCQ solution at times 0 and t, respectively.

Model fitting

The COD removal efficiency (η_{COD}) was modeled by a third-order polynomial (Eq. (5)) as function of density current (X_1), initial power of hydrogen (X_2), and stirring speed (X_3).

$$\begin{aligned}\eta_{COD} = {} & \gamma_0 + \gamma_1 x_1 + \gamma_2 x_2 + \gamma_3 x_3 + \gamma_{11} x_1^2 + \gamma_{22} x_2^2 + \gamma_{33} x_3^2 \ldots \\ & + \gamma_{111} x_1^3 + \gamma_{222} x_2^3 + \gamma_{333} x_3^3 + \gamma_{12} x_1 x_2 + \gamma_{13} x_1 x_3 + \gamma_{23} x_2 x_3 \ldots \\ & + \gamma_{123} x_1 x_2 x_3 + \gamma_{112} x_1^2 x_2 + \gamma_{113} x_1^2 x_3 + \gamma_{122} x_1 x_2^2 + \gamma_{133} x_1 x_3^2 \ldots \\ & + \gamma_{223} x_2^2 x_3 + \gamma_{233} x_2 x_3^2\end{aligned} \tag{5}$$

where (η_{COD}) is the COD model response, γ values are the coefficients of the polynomial, and x_i are the encrypted independent variables according to Eq. (1). The γ values were estimated by the stepwise regression method in the Design Expert ® V.10.0 software package.

Accuracy of the model

The accuracy of the adjusted polynomial to the experimental data was established by the determination coefficient (R^2, see Eq. (6)) [49], root mean square error (RMSE, see Eq. (7)) [50], and mean square error (MSE, see Eq. (8)) [51]. To achieve a very good model fitting, a low value of the error metrics is desirable.

$$R^2 = \frac{\sum_{i=1}^{n} \left(\eta_{exp,i} - \overline{\eta}_{\exp}\right)\left(\eta_{\text{mod }el,i} - \overline{\eta}_{\text{mod }el}\right)}{\sqrt{\sum_{i=1}^{n} \left(\eta_{exp,i} - \overline{\eta}_{\exp}\right)^2 \sum_{i=1}^{n} \left(\eta_{\text{mod }el,i} - \overline{\eta}_{\text{mod }el}\right)^2}} \tag{6}$$

$$RMSE = \sqrt{\frac{1}{n} \sum_{i=1}^{n} \left(\frac{\eta_{exp,i} - \eta_{\text{mod }el,i}}{\eta_{exp,i}}\right)^2} \tag{7}$$

$$MSE = \frac{1}{n} \sum_{i=1}^{n} \left(\eta_{exp,i} - \eta_{\text{mod }el,i}\right)^2 \tag{8}$$

where n is the number of experimental data points, $\eta_{\exp}$ is the experimental response, η_{model} is the modeled response, $\overline{\eta}_{\exp}$ and $\overline{\eta}_{\text{mod }el}$ are the average values of the experimental and model values, respectively.

Optimization process

The objective function of the non-convex constrained optimization problem was to maximize the COD removal efficiency (η_{COD}, third-order polynomial (Eq. (5))) subject to convex constraints ($x_i^2 \le \alpha^2,\ i = 1,\ 2,\ and\ 3$), where η_{COD} is a non-convex function (see Eq. (5)) and α represents the rotatability of the central composite design (CCD). The non-convex constrained optimization problem of the COD removal efficiency (η_{COD}) is written in standard form as shown by Eq. (9).

$$\begin{aligned} &Min \quad -\eta_{COD}(x_1, x_2, x_3) \\ &s.t. \\ &\quad x_1^2 \le \alpha^2 \\ &\quad x_2^2 \le \alpha^2 \\ &\quad x_3^2 \le \alpha^2 \\ &\alpha = 1.68 \end{aligned} \tag{9}$$

The optimal point of the non-convex constrained problem (Eq. (9)) was found employing three different algorithms (e.g., "active set," "sequential quadratic programming," and "interior-point"). To make easy this assignment, the *Toolbox* "fmincon" of MATLAB R2017a ® software package (License number: 1082300; Multion Consulting, S.A. de C.V, Calz, Mexico from MathWorks) was adopted. Also, an algorithm to solve the non-convex optimization problem assumed by Eq. (9) is accessible in the supported material (see Table S1).

Energy consumption and operating cost

The total energy consumption (*EC* (kW h)) for the electrochemical oxidation of HCQ was computed in terms of electricity consumed by the BDD electrodes ($E_{\text{electrodes}}$), by the stirrer (E_{stirrer}), and by the pump used to recirculate the cooling water ($E_{\text{pump, heat}}$) of the cooling systems, such as shown by Eqs. (10) to (13),

$$E_{electrodes} = U \times j \times a \times t \tag{10}$$

$$E_{stirrer} = P_{stirrer} \times t \tag{11}$$

$$E_{pump,\ heat} = P_{pump,\ heat} \times t \tag{12}$$

$$EC = E_{electrodes} + E_{stirred} + E_{pump,\ heat} \tag{13}$$

where U is the average cell potential (6.7 V), a is the electrode surface (20 cm^2), j is the applied current density (46.36 mA cm^{-2}), t is the electrolysis time (5 h), P_{stirrer} is the supplier catalog nominal power (0.02 kW) for stirring, and $P_{\text{pump, heat}}$ is the supplier catalog nominal power (0.123 kW) for the cooling system pump.

The total operating cost (OC (USD$)) is the sum of the total electricity price and the electrolyte price as denoted by Eq. (14).

$$OC = \xi \times EC + \phi \times m_{electrolyte} \tag{14}$$

where ξ is the electricity price (0.049 USD$/kW h, based on 1 USD$ (MXN 17.01) $^{-1}$), ϕ is the price of the electrolyte (0.8 USD$ kg^{-1}), and $m_{\text{electrolyte}}$ is the used electrolyte mass (0.0085 kg).

Results and discussions

Linear and cyclic voltammetry study

Linear and cyclic voltametric measurements were employed to study the electrochemical behavior of HCQ on the Nb/BDD electrode. Figure 2a shows the linear polarization curve of Na_2SO_4 (black line) and Na_2SO_4 + HCQ (red line) with BDD anode at 50 mV s^{-1} as scan rate. The curves (black and red lines) show that oxygen evolution potential starts at approximately + 1.8 V versus Ag/AgCl when no HCQ is presenting in water (Na_2SO_4), and thus, it is an insignificant electrocatalyst for the oxygen evolution reaction and this in concordance with that reported in [52]. While Na_2SO_4 + HCQ presents a well-defined peak at + 1.37 V before the oxygen evolution reaction, which corresponds to oxidation of HCQ by the production of hydroxyl radicals ($OH^{\bullet}$) and other oxidants species ($SO_4^{\bullet-}$ and $S_2O_8^{2-}$) in agreement with [53–55]. Figure 2b shows the cyclic voltammetry of Na_2SO_4 (black line) and Na_2SO_4 + HCQ (red line) with BDD anode at 50 mV s^{-1} as scan rate. Figure 2b exhibits a typical behavior of a non-reversible system when water contains HCQ with a well-defined peak at around + 1.37 V, which suggests that the HCQ is directly oxidized at the BDD electrode surface. Also, when the potential is increasing, a nonsmoothed current signal was observed after the peak at + 1.37 V, which may indicate that there is no remarkable signal of the oxidation by-products from HCQ in contrast with the reported results in [52]. Furthermore, the oxidation peaks (+ 1.37 V) of the electrolyte coincide with the oxidation peak of the HCQ, indicating that indirect oxidation of HCQ can be attained by $OH^{\bullet}$, $SO_4^{\bullet-}$, and $S_2O_8^{2-}$ [53, 56, 57].

Model fitting

In this work, the Design Expert ® V.10.0 software package was adopted to perform the CCRD, model fitting, and ANOVA analysis. To model the COD removal efficiency (η_{COD}), 17 assays of the CCRD were employed (Table S2). Trials 2, 5, 7, 9, 10, 12, 16, and 17 are factorial points; trials 4, 6, 11, 13,14, and 15 are axial points; trials 1, 3, and 8 are central points. The mean experimental values of η_{COD} for all assays are reported in Fig. 3. Also, in Fig. 3, it can be observed that the COD removal efficiency goes from 29.63 to 75.86%. It is worth mentioning that all trials were replicated by triplicate. Therefore, the design matrix and the mean COD removal efficiency (η_{COD}) data with their respective standard deviation for each trial are presented in Table S2.

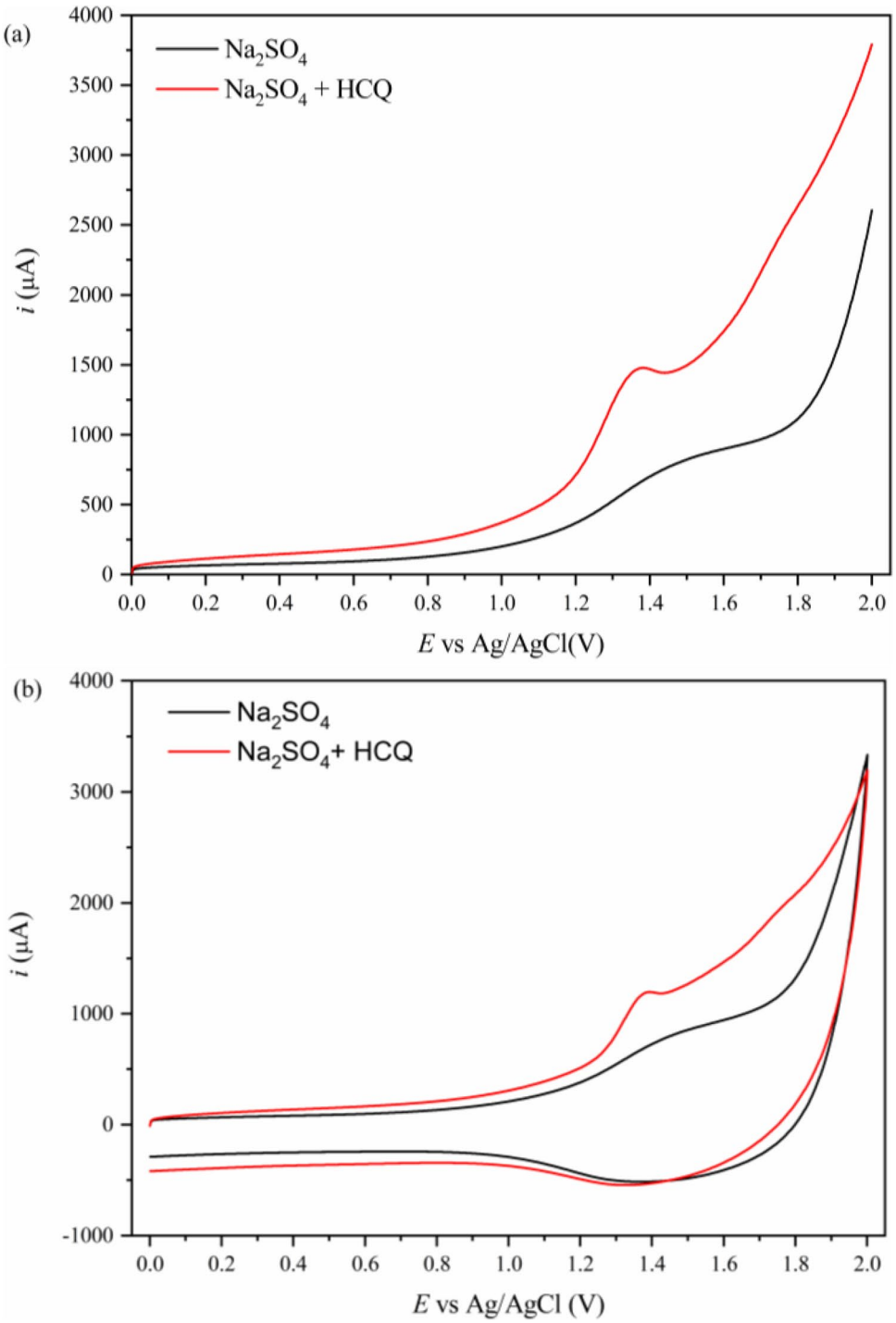

Fig. 2 **a** Polarization curve obtained for a 50 mg L^{-1} HCQ in 0.1 M Na_2SO_4 solution at anodic BDD electrode; **b** cyclic voltammogram obtained for a 50 mg L^{-1} HCQ in 0.1 M Na_2SO_4 solution at anodic BDD electrode. Potential scan rate: 50 mV $s.^{-1}$

The found relationship between η_{COD} and the operational factors (x_1, x_2, and x_3) fits a reduced third-order polynomial like Eq. (15).

Equation in encrypted factors,

$$\eta_{COD} = 54.03 + 13.74x_1 + 2.28x_2 + 5.98x_3 + 7.28x_1x_2 - 4.75x_1x_3 \ldots + 4.13x_2x_3 - 3.35x_2^2 + 3.74x_3^2 - 9.34x_1^2x_3 - 12.58x_1x_2^2 \quad (15)$$

The γ_0 (54.03) value corresponds to the overall average response (η_{COD}) of all trials. The variance inflation factors (VIF) for $\gamma_1, \gamma_2, \gamma_3, \gamma_{12}, \gamma_{13}, \gamma_{23}, \gamma_{22}, \gamma_{33}, \gamma_{113}$, and γ_{122} are 2.41, 1.00, 2.141, 1.00, 1.00, 1.00, 1.05, 1.05, 2.41, and 2.41, respectively. In this case study, the terms x_2, x_1x_2, x_1x_3, and x_2x_3 are orthogonal since their VIF values are 1. Also, the terms $x_1, x_3, x_2^2, x_3^2, x_1^2x_3$, and $x_1x_2^2$ are multicollinear because all VIF values are greater than 1. Furthermore, a higher VIF

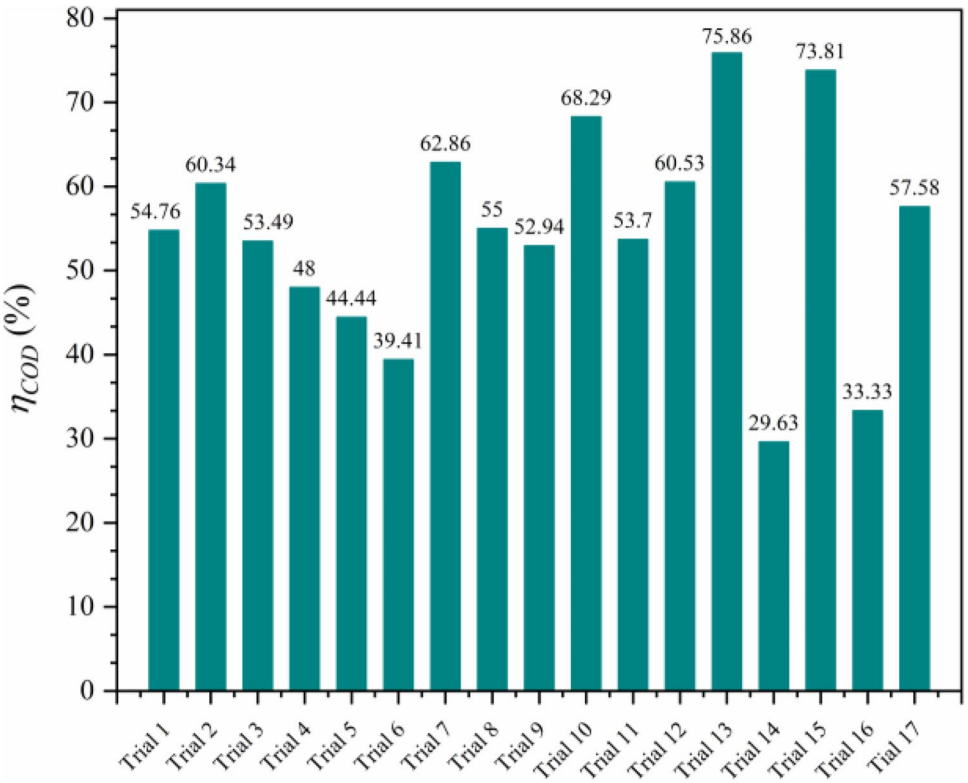

Fig. 3 Response values of the CCRD

value than 1 indicates a serious correlation of factors. As a rough rule, VIFs lower than 10 are acceptable.

Additionally, the positive sign before of $\gamma_1, \gamma_2, \gamma_3, \gamma_{12}, \gamma_{23}$, and, γ_{33} values suggests a positive effect on η_{COD}; while the negative sign of $\gamma_{12}, \gamma_{22}, \gamma_3, \gamma_{13}$, and, γ_{122} suggests a negative effect on η_{COD} [58].

Analysis of variance (ANOVA)

Table 4 displays the model fit statistics with $R^2 = 0.9906$, adjusted-$R^2 = 0.9749$, modeled-$R^2 = 0.8286$, std dev = 2.02%, mean = 54.35%, adequate precision = 28.4071, and C.V. (%) = 3.72. The determination

Table 4 Reduced third-order polynomial ANOVA for optimum COD removal efficiency

Source	Sum of squares	Degree of freedom	Mean square	*F-value*	*P-value*	Remark
Model	2586.46	10	258.650	63.19	< 0.0001	**Significant**
x_1	1068.61	1	1068.610	261.08	< 0.0001	
x_2	71.26	1	71.260	17.41	0.0059	
x_3	202.21	1	202.210	49.40	0.0004	
x_1x_2	423.55	1	423.550	103.48	< 0.0001	
x_1x_3	180.41	1	180.410	44.08	0.0006	
x_2x_3	136.37	1	136.370	33.32	0.0012	
x_2^2	138.35	1	138.350	33.80	0.0011	
x_3^2	172.94	1	172.940	42.25	0.0006	
$x_1^2x_3$	289.07	1	289.070	70.62	0.0002	
$x_1x_2^2$	524.25	1	524.250	128.08	< 0.0001	
Residuals	24.56	6	4.090			
Lack of fit	23.24	4	5.810	8.82	0.104	**Not significant**
Pure error	1.32	2	0.658			
Cor total	2611.01	16				

$R^2 = 0.9906$; adjusted-$R^2 = 0.9749$; modeled-$R^2 = 0.8286$; std dev = 2.02%; mean = 54.35%; adequate precision = 28.4071; C.V. (%) = 3.72

coefficient (R^2) is close to unit, thus indicating that the model fitted is in very good agreement with the experimental data [59] as this is confirmed with the parity plot shown in Fig. 4a.

The modeled-R^2 is in reasonable agreement with the adjusted-R^2 since the difference (0.1463) is less than 0.2. The F-value (63.19) implies that there is an adequate signal-to-noise ratio with only a 0.01% chance that noise could

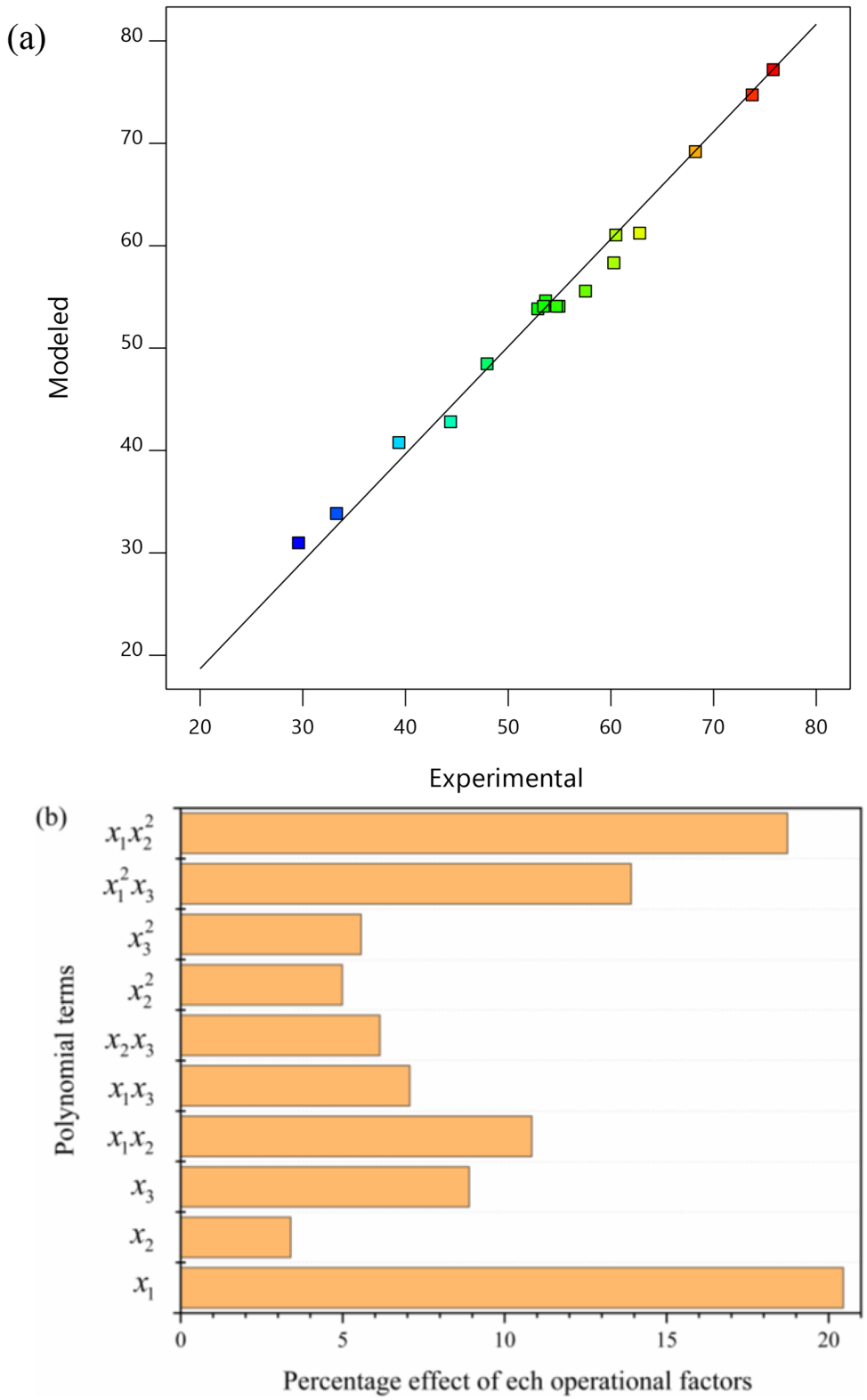

Fig. 4 **a** Parity plot; **b** Pareto plot

affect model accuracy. Also, the p-value (0.0001) confirms that the chosen reduced third-order polynomial is significantly evidenced for modeling the degree of interactions and relative impact of the removal efficiency of hydroxychloroquine parameters: current density (x_1), initial power of hydrogen (x_2), and stirring speed (x_3). Furthermore, the RMSE (0.0460) and MSE (0.0021) are close to 0, indicating that the reduced fitting third-order polynomial agrees very well with experimental data [60, 61].

The *lack of fit F-value* (8.82) implies that the lack of fit is not significant relative to the pure error with only 10.44% chance that an F-value this large could occur due to noise. Also, the $x_1, x_2, x_3, x_1x_2, x_1x_3, x_2x_3, x_2^2, x_3^2, x_1^2x_3, x_1x_2^2$ are significant model terms because all p-values are less than 0.05. Furthermore, the fitting model can be used to navigate the design space because the adequate precision ratio value (28.407) is greater than 4 [62].

Pareto analysis was conducted by using Eq. (16) to evaluate the percentage effect of each polynomial term (P_i) on response η_{COD},

$$P_i = \left(\frac{\gamma_i}{\sum \gamma_i}\right) \times 100 \tag{16}$$

Figure 4b depicts the Pareto plot analysis. The exposed results in this figure suggest that the terms γ_1 (current density (mA cm^{-2})) and γ_{122} (current density (mA cm^{-2})$\times$(pH$_0$ (dimensionless))^2) give the largest effect: 20.46%, and 18.73% on η_{COD}, respectively. Also, the interaction term γ_{113} ((current density (mA cm^{-2}))$^2\times$(Ω (rpm))) gives a medium effect: 13.91% on η_{COD}. Besides, the rest of terms γ_2, γ_3, γ_{12}, γ_{13}, γ_{22}, and γ_{33}, contribute the lowest effect: 3.39%, 8.90%,10.83%, 7.07%, 4.99%, and 5.57% on η_{COD}, respectively.

Non-convex optimization of the removal efficiency of hydroxychloroquine

The non-convex constrained optimization problem to be solved is stated by Eq. (17). The optimal operating point observed is displayed in Table 5. A local maximum was attained when the non-convex constrained optimization problem (Eq. (17)) was solved by performing different numerical methods. The three numerical methods used find a single optimal operating point. For this non-convex-constrained optimization problem, the IP and AC methods are significantly faster than the SQP method since they solve the non-convex-constrained optimization problem in only one iteration.

$$\begin{aligned} Min \quad & -\left[\begin{array}{l} 54.03 + 13.74x_1 + 2.28x_2 + 5.98x_3 + 7.28x_1x_2 - 4.75x_1x_3 \ldots \\ +4.13x_2x_3 - 3.35x_2^2 + 3.74x_3^2 - 9.34x_1^2x_3 - 12.58x_1x_2^2 \end{array}\right] \\ s.t. \quad & \\ & x_1^2 \le (1.68)^2 \\ & x_2^2 \le (1.68)^2 \\ & x_3^2 \le (1.68)^2 \end{aligned} \tag{17}$$

Figure 5 shows the contour graphs of the COD removal efficiency (η_{COD}) by means of electrochemical treatment. In the electrochemical treatment of organic chemicals such as hydroxychloroquine, the pH plays a key role since it controls the hydroxyl radical formation [33] and is related the molecule ionization hinted by its pKa. In concordance, Fig. 5a reveals the pH effect and its interaction with current density. Thus, it can be observed that high η_{COD} is achieved when j is increased if pH is kept close to 8. This suggests that around this pH, the oxidation of organic compounds might be mainly through direct electron transfer at the electrode surface. It is important to note that a similar η_{COD} (~74) is achieved either at low pH values (< 2) or high pH values (> 13) and relatively low current density (j < 35 mA cm^{-2}). This can be due to the presence of ozone (O_3), which has been demonstrated [63] to be produced with the same electrodes and supporting electrolyte. Depending on pH, O_3 can participate in direct oxidations at acidic pH [64] and in the case of chlorinated aromatic compounds, this proceeds at the chlorine position [65], thus producing other chlorine species that might also participate in the oxidation process. Nevertheless, when using BDD electrodes, it has also been demonstrated that the oxidation via O_3 is not superior to that via hydroxyl radicals. Under alkaline conditions, the participation of ozone in the oxidation process is indirect since the interaction with the hydroxyl ions is preferred, thus favoring the hydroxyl radical concentration in solution [64].

Figure 5b shows that η_{COD} increases as the Ω decreases, indicating that the pollutant travels (by diffusion) easily from

Table 5 Solved non-convex constrained optimization of η_{COD} employing different numerical methods

η_{COD} (%)	Method	Iteration	j (mA cm^{-2})	pH$_0$	Ω (rpm)	Characterization
85.551	IP	1	46.360	12.04	583.999	Local maximum
85.552	AC	5	46.366	12.04	584.000	Local maximum
85.552	SQP	1	46.360	12.04	584.000	Local maximum

IP, interior-point; *SQP*, sequential quadratic programming; *AC*, active set

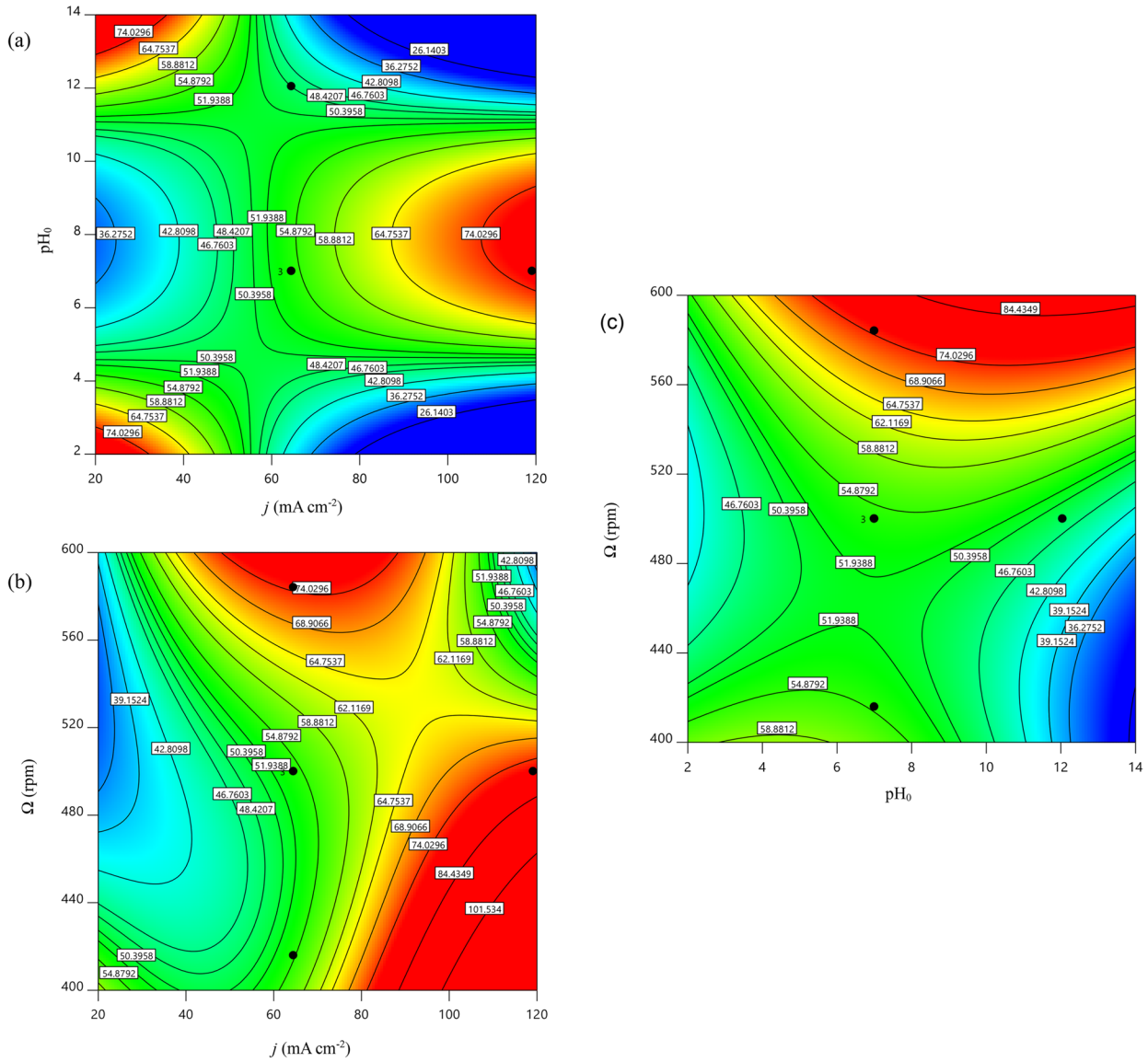

Fig. 5 **a** 2D plot effect of initial pH and j (mA cm-^{2}) on η_{COD}, Ω of 584 rpm and 5 h; **b** 2D plot effect of Ω (rpm) and j (mA cm^{-2}) on η_{COD}, pH_0 of 12.04; **c** 2D plot effect of Ω (rpm) and initial pH on η_{COD}, j of 46.36 mA cm^{-2}. Treatment time for all experiments was 5 h

the bulk to the electrode surface where there is a considerable amount of hydroxyl radicals (see Eq. (18)) able to react with the organic pollutant,

$$BDD + H_2O \rightarrow BDD(HO^{\bullet}) + H^{+} + e^{-} \quad (18)$$

Also, high η_{COD} is achieved when j is increased if the Ω is kept around 440 rpm. From Fig. 5c, it can be seen that η_{COD} increases as Ω increases. This suggests the process is being mass-transfer controlled and the resistance to this phenomenon is being reduced when the stirring speed increases. Similarly, high η_{COD} is attained as the pH decreases, indicating that hydroxyl radials ($OH^{\bullet}$) and hydroxyl anions (OH^{-}) were produced at the electrode surface. In this study, high η_{COD} is achieved because a high amount of $OH^{\bullet}$ is produced at acid and basic (pH ≥ 10) conditions directly and indirectly (by oxidation of OH^{-}), favoring the oxidation of pollutants [66].

Finally, the shapes of the contour plots in Fig. 5 depict a hyperbolic function, indicating that the optimal operating point is cataloged as a saddle point. Besides, as the unique optimal operating point was found, the local maximum also can be called a global maximum. Furthermore, the saddle point theorem [67] indicates that if there exists a saddle point as the solution to the minimization-constrained problem, it can be considered an optimal point since the existence of a saddle point is a sufficient condition assuming Karush–Kuhn–Tucker conditions.

Model verification

To confirm the optimal operating point previously found, a series of three complementary trials were performed under optimal operating variables established by non-convex optimization; computed and experimental values are displayed in Table 5. The relative error (6.47%) presented in Table 6 indicates a very good approximation of the optimal operating point by non-convex optimization. Thus, the maximum COD removal efficiency was 85.55% at a pH_0 of 12.04, a j of 46.36 mA cm^{-2}, and a Ω of 584 rpm within 5 h of electrochemical treatment.

Total operating cost

The total operating cost was computed as a function of energy consumption and the used mass of the electrolyte according to the set of Eqs. (10) to (13). Thus, the energy consumption was 0.746 kW h at a cost of 0.04 USD$ per 0.6 L of volume treated (or 0.067 USD$ L^{-1}) when the BEC operates under optimal operating conditions (j of 46.36 mA cm^{-2}, pH_0 of 12.04, and Ω of 584 rpm within 5 h of electrochemical treatment). It is worth mentioning that this research is the only one that reports the associated cost (see Table 7).

A TOC analysis was carried out according to the methodology described in the "Chemical analysis" section. The initial and final TOC values were 25.54 mg L^{-1} and 12.26 mg L^{-1}, respectively, accomplishing a TOC removal efficiency of 52.5% at 5 h of electrochemical treatment.

Table 6 The optimal operating point of the COD removal efficiency

Optimal point		Response η_{COD} (%)
j (mA cm^{-2}):	46.36	
pH_0:	12.04	
Ω (rpm):	584.00	
Modeled		85.55
Mean experimental		80.35 ± 0.34
Relative error (%)		6.47

Kinetic models

The electrochemical process employed here was carried out under galvanostatic conditions, where the electrochemical degradation of organic pollutants employing BDD anodes depends mainly on the production of $OH^{\bullet}$ [68]. Hence, it can be assumed that the reaction responsible for the degradation of organic pollutants (e.g., HCQ) is given by the $OH^{\bullet}$ on the BDD anode surface; a pseudo-first-order kinetic model was established to fit the experimental data following Eq. (19) according to reported in [69, 70].

Also, pseudo-first-order (see Eq. (20)) and pseudo-zero-order (see Eq. (21)) kinetic models for COD removal efficiency and TOC abatement, respectively, were employed to model the experimental data.

$$\frac{dC_{HCQ}}{dt} = -\underbrace{kC_{OH\cdot}}_{k_{app}} C_{HCQ} = -k_{app}C_{HCQ} \tag{19}$$

Table 7 Electrochemical degradation of HCQ under different electrolysis treatments

Operating environment	EL	V (L)	Main results					Ref
	Ca/An		η_{HCQ} (%)	η_{COD} (%)	η_{TOC} (%)	EC (kWhL^{-1})	OC (USD$$L^{-1}$)	
C_{HCQ} = 50 mg L^{-1} on 0.1 M de Na_2SO_4, pH_0 = 12.04, j = 46.36 mA cm^{-2}, Ω = 584 rpm, t = 5 h, and area = 20 cm^2	*/*	0.6	99.5	85.55	52.5	1.24	0.067	This work
C_{HCQ} = 250 mg L^{-1} on 0.05 M de Na_2SO_4, pH_0 = 7.1, j = 20 mA cm^{-2}, Q = 3.3 L min^{-1}, t = 5 h, and area = 78 cm^2	SS/*	0.6	100	—	82.0	0.102	—	[42]
C_{HCQ} = 26.8 mg L^{-1} on 0.1 M de H_2SO_4, pH_0 = 7.6, j = 45 mA cm^{-2}, Q = 3.3 L min^{-1}, t = 5 h, and area = 13.5 cm^2	Ti/*	0.25	100	84.00	—	5.0	—	[82]
C_{HCQ} = 200 mg L^{-1} on 0.05 M de Na_2SO_4, pH_0 = 7, j = 20 mA cm^{-2}, Ω = 200 rpm, and t = 3 h	SS/**	0.25	95.8	77.60	82.94	0.038	—	[80]
C_{HCQ} = 2170 mg L^{-1} on 2.0 M Acetate buffer, pH = 5.0, j = 6 mA cm^{-2}, Ω = 300 rpm, t = 3 h, and area = 4.5 cm^2	SS/***	0.05	94.2	68.00	—	—	—	[83]

EL electrodes, *Ca* cathode, *An* anode, *SS* stainless steel; *, *BDD*; **, Ti/(Ti, Zr)N/PbO_2-2.0; ***, CF/β-PbO_2-ZrO_2-MoO_x

$$\frac{dC_{COD}}{dt} = -k_{app,\ COD} C_{COD} \tag{20}$$

$$\frac{dC_{TOC}}{dt} = -k_{app,\ TOC} \tag{21}$$

The abatement in the absorbance maximum band of HCQ (343 nm) was observed in Fig. 6a, as a function of electrolysis time. The behavior shown in this figure indicates that the electrochemical degradation of HCQ forms another simple organic molecule since the $OH^{\bullet}$ attacks the chemical structure of HCQ. The determination of by-products was not measured because it is outside the scope of this investigation. Additionally, the presented behavior in Fig. 5c suggests a constant production of $OH^{\bullet}$. It is worth mentioning that Fig. 5a only includes profiles of absorbance from $t = 0$ to $t = 4$ h because a degradation efficiency of HCQ achieves 99.45% at 4 h and the profiles of absorbance will be superposing for reaction times from 5 to 8 h.

The behavior observed in Fig. 6b, c, and d discloses a satisfactory pseudo-first-order, pseudo-first-order, and pseudo-zero-order kinetic rate execution for degradation of HCQ, COD removal, and TOC removal, respectively. Performing a linear regression analysis, the k_{app}, $k_{app,\ COD}$, and $k_{app,\ TOC}$ values were 1.21 h^{-1}, 0.26 h^{-1}, 2.65 mg L^{-1} h^{-1}, respectively, with determination coefficients (R^2) values of 0.9911, 0.9711, and 0.9886, indicating high correlation because the values of R^2 are close to 1 [59]. It is worth stating that the reported apparent degradation kinetic constant (k_{app}) here can be called as a global oxidation constant because the electro-oxidation of the intermediates by the $OH^{\bullet}$ through reaction time were not differentiated for its determination.

A faster HCQ elimination (94.5%) in the first 2 h of the electrochemical treatment was observed (see Fig. S1)

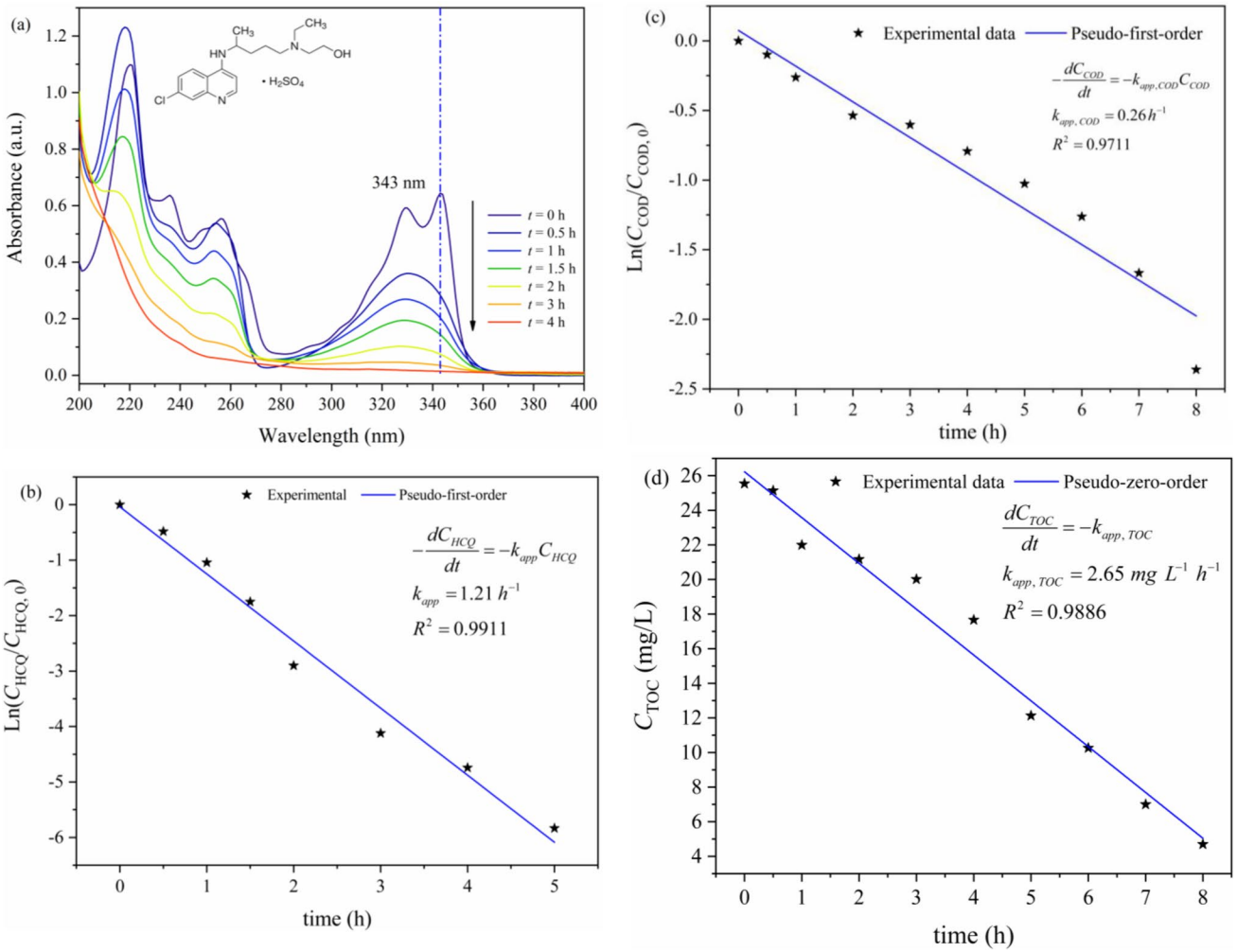

Fig. 6 **a** UV-Visible spectra for the HCQ solution at different electrolysis times; **b** Kinetic analysis for the pseudo-first-order model for HCQ degradation; **c** Kinetic analysis for the pseudo-first-order model for COD abatement; **d** Kinetic analysis for the pseudo-zero-order model for electrochemical mineralization of HCQ. C_{HCQ} = 50 mg L^{-1} on 0.1 M de Na_2SO_4, pH_0= 12.04, j = 46.36 mA cm^{-2}, Ω = 584 rpm, and t= 5 h

in concordance with the reported in [42]. This behavior is attributed to hydroxyl radicals formed on the Nb/BDD electrode surface, as described by Eq. (18).

Although hydroxyl radicals are the dominant oxidant species, a possible formation of persulfate ions ($S_2O_8^{2-}$) and sulfate radical ($SO_4^{\bullet-}$) on the Nb/BDD electrodes is due to the use of the sodium sulfate as an electrolyte [42, 71–73], according to Eqs. (22) to (27).

$$SO_4^{2-} + SO_4^{2-} \rightarrow S_2O_8^{2-} + 2e^- \tag{22}$$

$$SO_4^{\bullet-} + SO_4^{\bullet-} \rightarrow S_2O_8^{2-} \tag{23}$$

$$SO_4^{-} + e^- \rightarrow SO_4^{\bullet-} \tag{24}$$

$$SO_4^{-} + OH^{\bullet} \rightarrow SO_4^{\bullet-} + H^+ \tag{25}$$

$$S_2O_8^{2-} + e^- \rightarrow SO_4^{\bullet-} + SO_4^{2-} \tag{26}$$

$$S_2O_8^{2-} + \Delta\ ohmic\ heating \rightarrow 2SO_4^{\bullet-} \tag{27}$$

Also, a recombination of $SO_4^{\bullet-}$ with water to form hydroxyl radicals can be expected, according to Eq. (28). This reaction (Eq. (28)) proceeds in favor of the removal of persistent organic pollutants such as the HCQ.

$$SO_4^{\bullet-} + H_2O \rightarrow OH^{\bullet} \tag{28}$$

This electrochemical proposed treatment herring has been performed at 25 °C with a concentration of electrolyte support of 0.1 M, indicating that the degradation effect by sulfate radical and persulfate ion on the electrooxidation of HCQ is low concerning hydroxyl radicals formed on the BDD electrodes [74] in concordance with do the results reported in [71, 75], where comments that there is not enough evidence that the $S_2O_8^{2-}$ and $SO_4^{\bullet-}$ are formed at low temperatures (< 40 °C) since when BDD anode is employed heat addition is needed [76]. Similarly, there is not enough evidence that high concentrations of Na_2SO_4 (> 0.05 M) produce a high amount of $S_2O_8^{2-}$ and $SO_4^{\bullet-}$ when BDD electrodes are used. Finally, a recombination of $SO_4^{\bullet-}$ with $S_2O_8^{2-}$ could be given if there is an excess of $SO_4^{\bullet-}$ present in the aqueous solution [77], as is described by Eq. (29). This could play against the removal of persistent organic compounds. There is no evidence in this study that the sulfate radical and persulfate ion control the removal of HCQ in a similarly way as described in [42] because the electrochemical removal of the HCQ was carried out at alkaline conditions (pH of 12.04). Meanwhile, the sulfate radicals are favored in an acid medium is in agreement with reference [78]. This is supported by the polarization curve and the cyclic voltammogram (Fig. 2), which does not show any intermediate formation in contrast with the reported in [52]. According to the literature, the electrochemical process leads to the formation of stable carboxylic acids such as maleic, formic, acetic, malonic, oxamic, and oxalic acids [79]. Particularly, the electrochemical degradation of the HCQ, the expected intermediates when a similar Nb/BDD anode was employed are 7-chloro-4-quinolinamine, oxamic, and oxalic acids under acid conditions [42].

$$SO_4^{\bullet-} + S_2O_8^{2-} \rightarrow SO_4^{2-} + S_2O_8^{2-\bullet} \tag{29}$$

The results presented in this manuscript were compared with literature related to electrochemical degradation of HCQ (see Table 7). High degradation efficiency was attained in all literature reports including the results of the current work since are higher than 94%. In this work, high COD removal efficiency (85.55%) was achieved. TOC removal efficiency in this work (52.5%) is lower than that in reference [42] (82%), but the area of electrodes employed in reference [42] (78 cm^2) is approximately four times that used in this study (20 cm^2). Therefore, the contact area to react with the pollutant molecule in Ref. [42] is higher (78 cm^2) than the contact area (20 cm^2) employed in this study. Also, the cell configuration of Ref. [42] provides a higher mass transfer coefficient than the cell configuration used in this study. Even that Ref. [80] achieves the highest TOC removal efficiency (82.94%) than that attained in this work (52.5%), the volume of treated waste solution of HCQ in Ref. [80] is approximately 2.5 less than used in the current study, and this may be the cause for the lower TOC removal efficiency attained in this work. It is important to mention that this manuscript is the only one that performs the optimization of electrochemical degradation of HCQ and provides the associated cost (0.067 USD$ L^{-1}) at optimal operating conditions. Additionally, it can be noted that the current density applied in this study is higher (46.36 mA cm^{-2}) than in other studies [42, 80] since here two BDD electrodes have been employed. Hence, the BDD anode is considered a semiconductor causing an increase in current density consumption [81]. Nevertheless, the energy consumption used in Ref. [82] is higher (5 kW h L^{-1}) than in this research (1.24 kW h L^{-1}). Finally, even though Ref. [83] uses a higher concentration of HCQ (2170 mg L^{-1}) than this work (50 mg L^{-1}), the volume treated here is 12 times that used in Ref. [83]. Based on the results reported in this research, the applied electrochemical wastewater treatment employed is suitable for HCQ removal.

Future work

Electrochemical wastewater treatment for drug contaminants such as HCQ is a green and promising technology since offers high efficiency and integrates renewable energies (e.g.,

aero generators, solar panels, hydroelectric plants, and others). Another important aspect to punch-up as preferable to the electrochemical process implies conducting the electrochemical plants scalable under a low-cost-effective perspective. Also, life cycle studies must be applied to evaluate the sustainability of the electrochemical wastewater processes.

Conclusions

Upon the results of this investigation, the ensuing conclusions are derived as follows:

- The potentiodynamic polarization study demonstrates an irreversible oxidation of the hydroxychloroquine on the Nb/BDD electrode surface.
- The electrochemical degradation of hydroxychloroquine was successfully driven by hydroxyl radicals in a batch electrochemical cell equipped with two BDD electrodes.
- The reduced third-order polynomial to model the COD removal efficiency (η_{COD}) in a batch electrochemical cell equipped with two BDD electrodes was established as function j (x_1), pH_0 (x_2), and Ω (x_3). Also, the current density was the most significant factor in η_{COD} and follows the stirred speed factor. This reduced third-order function in encrypted terms is
$$\eta_{COD} = 54.03 + 13.74x_1 + 2.28x_2 + 5.98x_3 + 7.28x_1x_2 - 4.75x_1x_3 \ldots$$
$$+4.13x_2x_3 - 3.35x_2^2 + 3.74x_3^2 - 9.34x_1^2x_3 - 12.58x_1x_2^2$$
- The optimization of operational parameters was successfully reached by the non-convex optimization method. A global maximum of η_{COD} (85.55%) was achieved under j of 46.36 mA cm^{-2}, pH_0 of 12.04, and Ω of 584 rpm within 5 h of electrolysis time, employing an EC of 1.24 kW h L^{-1} with an OC of 0.067 USD$ L^{-1}.
- Electrochemical degradation of the HCQ, COD removal, and TOC removal follows pseudo-first-order, pseudo-first-order, and pseudo-zero-order kinetic rates, respectively, when the batch electrochemical cell operates under optimal reaction conditions.
- The green process evaluated in the current research has a potential industrial use since has a low-cost (0.067 USD$ L^{-1}), low EC (0.7461 kW h), no additional chemicals must be added to carry out the electrochemical treatment, and the EC can be easily provided by photovoltaic cells with batteries.

Supplementary Information The online version contains supplementary material available at https://doi.org/10.1007/s10008-024-05962-y.

Acknowledgements The support of Derek Joe Brockett, an English professor at Universidad del Mar, is acknowledged for his support in correcting the English writing of this work. Finally, authors would like to thank the staff of the environmental and investigation laboratories for dedicating their time and effort to facilitate the materials to conduct this research work.

Funding The authors are grateful to Universidad del Mar for providing financial support for the research project CUP: 2II2104. Also, the authors (A.R.-M., E.P.-R., and R.N.) are grateful to the Mexican Council of Science and Technology (CONAHCyT) for the financial support through the Investigators National System program (SNII). Similarly, D.V.-H. thank CONAHCyT-Mexico for providing scholarship No. 809459 for his master's studies.

Declarations

Conflict of interest The authors declare no competing interests.

References

1. Dima A, Jurcut C, Arnaud L (2021) Hydroxychloroquine in systemic and autoimmune diseases: where are we now? Joint Bone Spine 88:105143. https://doi.org/10.1016/J.JBSPIN.2021.105143
2. Geleris J, Sun Y, Platt J et al (2020) Observational study of hydroxychloroquine in hospitalized patients with Covid-19. N Engl J Med 382:2411–2418. https://doi.org/10.1056/NEJMOA2012410/SUPPL_FILE/NEJMOA2012410_DISCLOSURES.PDF
3. Kargar F, Bemani A, Sayadi MH, Ahmadpour N (2021) Synthesis of modified beta bismuth oxide by titanium oxide and highly efficient solar photocatalytic properties on hydroxychloroquine degradation and pathways. J Photochem Photobiol A Chem 419:113453. https://doi.org/10.1016/J.JPHOTOCHEM.2021.113453
4. United Nations (2016) Sustainable Development Goals (SDG 6) | United Nations Western Europe. In: United Nations. https://unric.org/en/sdg-6/. Accessed 22 Jan 2024
5. Albornoz LL, Soroka VD, Silva MCA (2021) Photo-mediated and advanced oxidative processes applied for the treatment of effluents with drugs used for the treatment of early COVID-19: review. Environmental Advances 6:100140. https://doi.org/10.1016/j.envadv.2021.100140
6. Kuroda K, Li C, Dhangar K, Kumar M (2021) Predicted occurrence, ecotoxicological risk and environmentally acquired resistance of antiviral drugs associated with COVID-19 in environmental waters. Sci Total Environ 776:145740. https://doi.org/10.1016/J.SCITOTENV.2021.145740
7. Dabić D, Babić S, Škorić I (2019) The role of photodegradation in the environmental fate of hydroxychloroquine - ScienceDirect. Chemospherere 230:268–277
8. Martínez-Huitle CA, Rodrigo MA, Sirés I, Scialdone O (2023) A critical review on latest innovations and future challenges of electrochemical technology for the abatement of organics in water. Appl Catal B 328:. https://doi.org/10.1016/J.APCATB.2023.122430
9. Oturan MA (2021) Outstanding performances of the BDD film anode in electro-Fenton process: applications and comparative performance. Curr Opin Solid State Mater Sci 25:100925. https://doi.org/10.1016/J.COSSMS.2021.100925
10. Espinoza-Montero PJ, Alulema-Pullupaxi P, Frontana-Uribe BA, Barrera-Diaz CE (2022) Electrochemical production of hydrogen peroxide on boron-doped diamond (BDD) electrode. Curr Opin Solid State Mater Sci 26:100988. https://doi.org/10.1016/J.COSSMS.2022.100988
11. Queiroz J, Moura D, Santos E, et al (2020) Electrochemical incineration of short-chain carboxylic acids with Nb-supported boron

doped diamond anode: supporting electrolyte into the electro-generated oxidant species (Hydroxyl radicals, hydrogen peroxide and persulfate). Quim Nova 43:253–260. https://doi.org/10.21577/0100-4042.20170483
12. Martínez-Huitle CA, Panizza M (2018) Electrochemical oxidation of organic pollutants for wastewater treatment. Curr Opin Electrochem 11:62–71. https://doi.org/10.1016/J.COELEC.2018.07.010
13. Hu Z, Cai J, Song G et al (2021) Anodic oxidation of organic pollutants: anode fabrication, process hybrid and environmental applications. Curr Opin Electrochem 26:100659. https://doi.org/10.1016/J.COELEC.2020.100659
14. dos Santos AJ, Kronka MS, Fortunato GV, Lanza MRV (2021) Recent advances in electrochemical water technologies for the treatment of antibiotics: a short review. Curr Opin Electrochem 26:100674. https://doi.org/10.1016/J.COELEC.2020.100674
15. Salazar-Banda GR, de Santos G, OS, Duarte Gonzaga IM, et al (2021) Developments in electrode materials for wastewater treatment. Curr Opin Electrochem 26:100663. https://doi.org/10.1016/J.COELEC.2020.100663
16. Martínez-Huitle CA, Rodrigo MA, Sirés I, Scialdone O (2015) Single and coupled electrochemical processes and reactors for the abatement of organic water pollutants: a critical review. Chem Rev 115:13362–13407. https://doi.org/10.1021/acs.chemrev.5b00361
17. Pointer Malpass GR, de Jesus MA (2021) Recent advances on the use of active anodes in environmental electrochemistry. Curr Opin Electrochem 27:100689. https://doi.org/10.1016/J.COELEC.2021.100689
18. Herraiz-Carboné M, Santos A, Checa-Fernández A et al (2024) Removal of organochlorine pollutants from DNAPL-saturated groundwater using electrolysis with MMO anodes. Chem Eng J 486:150238. https://doi.org/10.1016/J.CEJ.2024.150238
19. Barisci S, Suri R (2023) Degradation of emerging per- and polyfluoroalkyl substances (PFAS) using an electrochemical plug flow reactor. J Hazard Mater 460:132419. https://doi.org/10.1016/J.JHAZMAT.2023.132419
20. Dehkordi NR, Knapp M, Compton P et al (2022) Degradation of dissolved RDX, NQ, and DNAN by cathodic processes in an electrochemical flow-through reactor. J Environ Chem Eng 10:107865. https://doi.org/10.1016/J.JECE.2022.107865
21. Cornejo OM, Murrieta MF, Castañeda LF, Nava JL (2020) Characterization of the reaction environment in flow reactors fitted with BDD electrodes for use in electrochemical advanced oxidation processes: a critical review. Electrochim Acta 331:135373
22. Cordeiro-Junior PJM, Lobato Bajo J, Lanza MRDV, Rodrigo Rodrigo MA (2022) Highly efficient electrochemical production of hydrogen peroxide using the GDE technology. Ind Eng Chem Res 61:10660–10669. https://doi.org/10.1021/ACS.IECR.2C01669/ASSET/IMAGES/LARGE/IE2C01669_0009.JPEG
23. Sandoval MA, Fuentes R, Pérez T et al (2021) Modelling and simulation of H_2–H_2O bubbly flow through a stack of three cells in a pre-pilot filter press electrocoagulation reactor. Sep Purif Technol 261:118235. https://doi.org/10.1016/J.SEPPUR.2020.118235
24. He Y, Zhang P, Huang H et al (2020) Electrochemical degradation of herbicide diuron on flow-through electrochemical reactor and CFD hydrodynamics simulation. Sep Purif Technol 251:117284. https://doi.org/10.1016/J.SEPPUR.2020.117284
25. Walsh FC, Arenas LF, de León CP (2021) Editors' choice—critical review—the bipolar trickle tower reactor: concept, development and applications. J Electrochem Soc 168:023503. https://doi.org/10.1149/1945-7111/ABDD7A
26. Mousset E, Trellu C, Olvera-Vargas H et al (2021) Electrochemical technologies coupled with biological treatments. Curr Opin Electrochem 26:100668. https://doi.org/10.1016/J.COELEC.2020.100668
27. Clematis D, Panizza M (2021) Electrochemical oxidation of organic pollutants in low conductive solutions. Curr Opin Electrochem 26:100665. https://doi.org/10.1016/J.COELEC.2020.100665
28. Arenas LF, Ponce de León C, Walsh FC (2020) Critical review—the versatile plane parallel electrode geometry: an illustrated review. J Electrochem Soc 167:023504. https://doi.org/10.1149/1945-7111/AB64BA
29. Castillo-Cabrera GX, Pliego-Cerdán CI, Méndez E, Espinoza-Montero PJ (2024) Step-by-step guide for electrochemical generation of highly oxidizing reactive species on BDD for beginners. Front Chem 11:1298630. https://doi.org/10.3389/FCHEM.2023.1298630
30. Rodríguez-Peña M, Natividad R, Barrera-Díaz CE, et al (2024) Current perspective of advanced electrochemical oxidation processes in wastewater treatment and life cycle analysis. Int J Electrochem Sci 100589. https://doi.org/10.1016/J.IJOES.2024.100589
31. Song J, Li W, Li Y et al (2019) Treatment of landfill leachate RO concentration by iron–carbon micro–electrolysis (ICME) coupled with H_2O_2 with emphasis on convex optimization method. Environmental Pollutants and Bioavailability 31:49–55. https://doi.org/10.1080/09542299.2018.1552086
32. Zhang B, Sun J, Wang Q et al (2017) Electro-Fenton oxidation of coking wastewater: optimization using the combination of central composite design and convex optimization method. Environ Technol 38:2456–2464. https://doi.org/10.1080/09593330.2016.1265591
33. Regalado-Méndez A, Zavaleta-Avendaño J, Peralta-Reyes E, Natividad R (2023) Convex optimization for maximizing the degradation efficiency of chloroquine in a flow-by electrochemical reactor. J Solid State Electrochem 27:3163–3176. https://doi.org/10.1007/S10008-023-05452-7/FIGURES/5
34. Hemavathi M, Varghese E, Shekhar S et al (2022) Robustness of sequential third-order response surface design to missing observations. Journal of Taibah University for Science 16:270–279. https://doi.org/10.1080/16583655.2022.2046398
35. Regalado-Méndez A, Ruiz M, Hernández-Servín JA et al (2020) Electrochemical mineralization of ibuprofen on BDD electrodes in an electrochemical flow reactor: numerical optimization approach. Processes 8:1666. https://doi.org/10.3390/PR8121666
36. Kumar A, Wu G, Ali MZ et al (2020) A test-suite of non-convex constrained optimization problems from the real-world and some baseline results. Swarm Evol Comput 56:100693. https://doi.org/10.1016/J.SWEVO.2020.100693
37. Hoseini N, Nobakhtian S (2018) A new trust region method for nonsmooth nonconvex optimization. Optimization 67:1265–1286. https://doi.org/10.1080/02331934.2018.1470175
38. Jorge N, Wright SJ (2006) Numerical optimization, 2nd edn. Springer, New York, NY
39. Henrion D, Lasserre JB (2004) Solving nonconvex optmization problems. IEEE Control Syst 24:72–83. https://doi.org/10.1109/MCS.2004.1299534
40. Boujelbane F, Nasr K, Sadaoui H et al (2022) Decomposition mechanism of hydroxychloroquine in aqueous solution by gamma irradiation. Chem Pap 76:1777–1787. https://doi.org/10.1007/S11696-021-01969-1/FIGURES/10
41. da Silva PL, Nippes RP, Macruz PD et al (2021) Photocatalytic degradation of hydroxychloroquine using ZnO supported on clinoptilolite zeolite. Water Sci Technol 84:763–776. https://doi.org/10.2166/WST.2021.265
42. Bensalah N, Midassi S, Ahmad MI, Bedoui A (2020) Degradation of hydroxychloroquine by electrochemical advanced oxidation processes. Chem Eng J 402:126279. https://doi.org/10.1016/J.CEJ.2020.126279

43. Alves da Silva AE, de Abreu PMB, Geraldes DC, de Oliveira NL (2021) Hydroxychloroquine: pharmacological, physicochemical aspects and activity enhancement through experimental formulations. J Drug Deliv Sci Technol 63:102512. https://doi.org/10.1016/J.JDDST.2021.102512
44. Mamontov E, Cheng Y, Daemen LL et al (2020) Effect of hydration on the molecular dynamics of hydroxychloroquine sulfate. ACS Omega 5:21231–21240. https://doi.org/10.1021/acsomega.0c03091
45. Khalafalla M, Belgacem CH, Ismail IA, Chaieb K (2021) Uv-vis and electrical impedance characterizations of the hydroxychloroquine-zinc complex in the phospholipid-like oleic acid phase. SSRN Electron J. https://doi.org/10.2139/ssrn.3870977
46. Maldonado S, Rodrigo M, Cañizares P et al (2020) On the degradation of 17-β estradiol using boron doped diamond electrodes. Processes 8:710. https://doi.org/10.3390/pr8060710
47. Peralta E, Ruíz M, Martínez G, et al (2018) Degradation of 4-chlorophenol in a batch electrochemical reactor using BDD electrodes. Int J Electrochem Sci 13:4625–4639. https://doi.org/10.20964/2018.05.21
48. Baird RW, Eaton AD, Rice EW (2017) Standard methods for the examination of water and wastewater, 23rd edn. American Public Health Association, Washington, DC
49. Mechati S, Zamouche M, Tahraoui H, et al (2023) Modeling and optimization of hybrid Fenton and ultrasound process for crystal violet degradation using AI techniques. Water 2023, Vol 15, Page 4274 15:4274.https://doi.org/10.3390/W15244274
50. Kim S, Kim YK (2004) Apparent desorption kinetics of phenol in organic solvents from spent activated carbon saturated with phenol. Chem Eng J 98:237–243. https://doi.org/10.1016/J.CEJ.2003.10.006
51. Karunasingha DSK (2022) Root mean square error or mean absolute error? Use their ratio as well. Inf Sci (N Y) 585:609–629. https://doi.org/10.1016/J.INS.2021.11.036
52. Medeiros de Araújo D, Dos Santos EV, Martínez-Huitle CA, De Battisti A (2022) Achieving electrochemical-sustainable-based solutions for monitoring and treating hydroxychloroquine in real water matrix. Appl Sci 12:699. https://doi.org/10.3390/app12020699
53. Divyapriya G, Nidheesh PV (2021) Electrochemically generated sulfate radicals by boron doped diamond and its environmental applications. Curr Opin Solid State Mater Sci 25:100921. https://doi.org/10.1016/J.COSSMS.2021.100921
54. Ganiyu SO, Martínez-Huitle CA, Oturan MA (2021) Electrochemical advanced oxidation processes for wastewater treatment: advances in formation and detection of reactive species and mechanisms. Curr Opin Electrochem 27:100678. https://doi.org/10.1016/J.COELEC.2020.100678
55. Ahmadi MF, da Silva ÁRL, Martínez-Huitle CA, Bensalah N (2021) Understanding the electro-catalytic effect of benzene ring substitution on the electrochemical oxidation of aniline and its derivatives using BDD anode: cyclic voltammetry, bulk electrolysis and theoretical calculations. Electrochim Acta 369:137688. https://doi.org/10.1016/J.ELECTACTA.2020.137688
56. Bensalah N, Faouzi Ahmadi M, Martinez-Huitle CA (2021) Electrochemical oxidation of 2-chloroaniline in single and divided electrochemical flow cells using boron doped diamond anodes. Sep Purif Technol 263:118399. https://doi.org/10.1016/J.SEPPUR.2021.118399
57. Martínez-Huitle CA, Brillas E (2021) A critical review over the electrochemical disinfection of bacteria in synthetic and real wastewaters using a boron-doped diamond anode. Curr Opin Solid State Mater Sci 25:100926. https://doi.org/10.1016/J.COSSMS.2021.100926
58. Peralta-Reyes E, Vizarretea-Vásquez D, Natividad R et al (2022) Electrochemical reforming of glycerol into hydrogen in a batch-stirred electrochemical tank reactor equipped with stainless steel electrodes: Parametric optimization, total operating cost, and life cycle assessment. J Environ Chem Eng 10:108108. https://doi.org/10.1016/J.JECE.2022.108108
59. Montgomery DC (2019) Design and Analysis of Experiments, 10th edn. Wiley, New York
60. Mequanient MB, Kebede HH (2023) Simulation of sediment yield and evaluation of best management practices in Azuari watershed, Upper Blue Nile Basin. H_2Open Journal 6:493–506. https://doi.org/10.2166/H2OJ.2023.159
61. Tyagi K, Rane C, Harshvardhan, Manry M (2022) Regression analysis. Artificial intelligence and machine learning for EDGE computing 53–63. https://doi.org/10.1016/B978-0-12-824054-0.00007-1
62. Aziz SQ, Aziz HA, Yusoff MS, Bashir MJK (2011) Landfill leachate treatment using powdered activated carbon augmented sequencing batch reactor (SBR) process: optimization by response surface methodology. J Hazard Mater 189:404–413. https://doi.org/10.1016/J.JHAZMAT.2011.02.052
63. Santana-Martínez G, Roa-Morales G, Gómez-Olivan L, et al (2021) Downflow Bubble Column Electrochemical Reactor (DBCER): in-situ production of H_2O_2 and O_3 to conduct Electroperoxone Process. J Environ Chem Eng 105148. https://doi.org/10.1016/j.jece.2021.105148
64. Natividad R, Hurtado L, Romero R, et al (2019) Nanostructured metallic oxides for water remediation. Engineering Materials 91–119. https://doi.org/10.1007/978-3-030-33745-2_4/COVER
65. Amado-Piña D, Roa-Morales G, Molina-Mendieta M, et al (2022) E-peroxone process of a chlorinated compound: oxidant species, degradation pathway and phytotoxicity. J Environ Chem Eng 108148. https://doi.org/10.1016/J.JECE.2022.108148
66. Marselli B, Garcia-Gomez J, Michaud P-A et al (2003) Electrogeneration of hydroxyl radicals on boron-doped diamond electrodes. J Electrochem Soc 150:D79. https://doi.org/10.1149/1.1553790/XML
67. Goh CJ, Yang XQ (1997) A sufficient and necessary condition for nonconvex constrained optimization. Appl Math Lett 10:9–12. https://doi.org/10.1016/S0893-9659(97)00075-X
68. Liu G, Zhang C, Zhou Y, Yan Q (2021) Insight into the overpotential and thermodynamic mechanism of hydroxyl radical formation on diamond anode. Appl Surf Sci 565:150559. https://doi.org/10.1016/J.APSUSC.2021.150559
69. Bany Abdelnabi AA, Al Theeb N, Almomani MA et al (2022) Effect of electrode parameters in the electro-production of reactive oxidizing species via boron-doped diamond under batch mode. Water Environ Res 94:e10830. https://doi.org/10.1002/WER.10830
70. Comninellis C, Kapalka A, Malato S et al (2008) Advanced oxidation processes for water treatment: advances and trends for R&D. J Chem Technol Biotechnol 83:769–776. https://doi.org/10.1002/JCTB.1873
71. Shin YU, Yoo HY, Ahn YY et al (2019) Electrochemical oxidation of organics in sulfate solutions on boron-doped diamond electrode: multiple pathways for sulfate radical generation. Appl Catal B 254:156–165. https://doi.org/10.1016/J.APCATB.2019.04.060
72. Cai J, Niu T, Shi P et al (2019) Boron-doped diamond for hydroxyl radical and sulfate radical anion electrogeneration, Transformation, and Voltage-Free Sustainable Oxidation. Small 15:1900153. https://doi.org/10.1002/SMLL.201900153
73. Wacławek S, Lutze HV, Grübel K et al (2017) Chemistry of persulfates in water and wastewater treatment: a review. Chem Eng J 330:44–62. https://doi.org/10.1016/J.CEJ.2017.07.132
74. Farhat A, Keller J, Tait S, Radjenovic J (2015) Removal of persistent organic contaminants by electrochemically activated

sulfate. Environ Sci Technol 49:14326–14333. https://doi.org/10.1021/acs.est.5b02705
75. Ganiyu SO, Martínez-Huitle CA (2019) Nature, mechanisms and reactivity of electrogenerated reactive species at thin-film boron-doped diamond (BDD) electrodes during electrochemical wastewater treatment. ChemElectroChem 6:2379–2392. https://doi.org/10.1002/CELC.201900159
76. Groenen Serrano K (2021) A critical review on the electrochemical production and use of peroxo-compounds. Curr Opin Electrochem 27:100679. https://doi.org/10.1016/J.COELEC.2020.100679
77. Zhi D, Lin Y, Jiang L et al (2020) Remediation of persistent organic pollutants in aqueous systems by electrochemical activation of persulfates: a review. J Environ Manage 260:110125. https://doi.org/10.1016/J.JENVMAN.2020.110125
78. Giannakis S, Lin KYA, Ghanbari F (2021) A review of the recent advances on the treatment of industrial wastewaters by sulfate radical-based advanced oxidation processes (SR-AOPs). Chem Eng J 406:127083. https://doi.org/10.1016/J.CEJ.2020.127083
79. Martínez-Huitle CA, Ferro S (2006) Electrochemical oxidation of organic pollutants for the wastewater treatment: direct and indirect processes. Chem Soc Rev 35:1324–1340. https://doi.org/10.1039/B517632H
80. Tang C, Cui D, Li Z et al (2023) Electrooxidation degradation of hydroxychloroquine in wastewater using a long-acting Ti-based PbO_2 anode with an arc-sprayed (Ti, Zr)N interlayer. Chemosphere 335:139074. https://doi.org/10.1016/J.CHEMOSPHERE.2023.139074
81. Regalado-Méndez A, Ramos-Hernández G, Natividad R, et al (2023) Parametric mathematical model of the electrochemical degradation of 2-chlorophenol in a flow-by reactor under batch recirculation mode. Water 2023, Vol 15, Page 4276 15:4276. https://doi.org/10.3390/W15244276
82. de Araújo DM, Dos Santos E V., Martínez-Huitle CA, De Battisti A (2022) Achieving electrochemical-sustainable-based solutions for monitoring and treating hydroxychloroquine in real water matrix. Applied Sciences (Switzerland) 12. https://doi.org/10.3390/app12020699
83. Ashrafi P, Nematollahi D, Shabanloo A et al (2023) A detailed electrochemical study of anti-malaria drug hydroxychloroquine: application of a highly porous 3D multi-metal oxide carbon felt/β-PbO_2-ZrO_2−MoO_x electrode for its electrocatalytic degradation. Electrochim Acta 458:142555. https://doi.org/10.1016/j.electacta.2023.142555